Braz J Phys (2014) 44:711–718
DOI 10.1007/s13538-014-0269-8

CONDENSED MATTER

Characterization of Zn-Doped $Ga_{0.86}In_{0.14}As_{0.13}Sb_{0.87}$

J. Díaz-Reyes · P. Rodríguez-Fragoso · J. G. Mendoza-Álvarez · J. S. Arias-Cerón · J. L. Herrera-Pérez · M. Galván-Arellano

Received: 10 May 2014 / Published online: 1 October 2014

Abstract Controlled doping of quaternary alloys of $Ga_{0.86}In_{0.14}As_{0.13}Sb_{0.87}$ with zinc is fundamental to obtain the p-type layers needed for the development of optoelectronic devices based on p–n heterojunctions. GaInAsSb epitaxial layers were grown by liquid phase epitaxy, and Zn doping was obtained by incorporating small Zn pellets in the growth melt. The chemical composition was obtained by X-ray dispersive energy microanalysis (EDX). The chemical composition homogeneity of the films was demonstrated by Raman scattering. Low-temperature photoluminescence (LT-PL) spectroscopy was used to study the influence of the Zn acceptor levels on optical properties of the epilayers. For the undoped sample, the LT-PL spectrum showed a narrow exciton-related peak centered at around 648 meV with a full width at half maximum (FWHM) of about 7 meV, which is evidence of the good crystalline quality of the layers. For higher Zn-doping, the LT-PL spectra show the presence of band-to-band and donor-to-acceptor transitions, which overlap as the Zn concentration increases. The band-to-band radiative transition (E_M) shifts to lower energies as Zn doping increases due to a band-filling effect as the Fermi level enters into the valence band, which might be used to estimate the hole concentration in the grown samples.

Keywords Novel materials and technological advances for photonics · III–V semiconductors compound growth · GaInAsSb semiconductors · Photoluminescence · Raman · EDS

1 Introduction

The alloy system $Ga_{1-x}In_xAs_{1-y}Sb_y$ is interesting for optoelectronic applications because its room-temperature band gap covers the extremely wide range from 1.43 to 0.10 eV. For a lattice matched to InP substrates, the energy band gap is nearly fixed, ranging from 0.74 to 0.78 eV. However, for a lattice matched to GaSb, the energy band gap varies between 0.73 and 0.29 eV, corresponding to the wavelength range from 1.7 to 4.3 μm. This is a very interesting wavelength range for anticipated future fiber optic communication systems. The development of new fibers, such as the heavy metal fluoride fibers, offers a possible reduction of one or two orders of magnitude in loss compared with conventional $Si0_2$ fibers. The minimum loss is expected to occur in the wavelength range from 2 to 4 μm [1]. Although, the alloy system $Ga_{1-x}In_xAs_{1-y}Sb_y$ is known for some time, it has received relatively little attention until recently because it is known to have a very large miscibility gap [2] with a critical temperature estimated to be 1467 °C. As was shown by Nakajima et al. [3], this restricts the range of solid alloys which can be grown by liquid phase epitaxy (LPE). Dolginov et al. [4] reported the LPE growth of alloys near GaSb, with values of x <0.2 and y >0.8. Kobayashi et al. [5] and Kano et al. [6] have studied the LPE growth of $Ga_{1-x}In_xAs_{1-y}Sb_y$ on GaSb substrates with x limited to the range <0.18. More recently, DeWinter et al. [7]

J. Díaz-Reyes (✉)
Centro de Investigación en Biotecnología Aplicada, Instituto Politécnico Nacional, Ex-Hacienda de San Juan Molino Km. 1.5. Tepetitla, Tlaxcala 90700, México
e-mail: joel_diaz_reyes@hotmail.com

P. Rodríguez-Fragoso · J. G. Mendoza-Álvarez · J. S. Arias-Cerón
Departamento de Física, CINVESTAV-IPN, Apartado Postal 14-740, México, D. F. 07000, México

J. L. Herrera-Pérez
UPIITA-IPN, Av. Instituto Politécnico Nacional 2580, Barrio La Laguna Ticomán, Deleg. Gustavo A. Madero, México, D. F. 07340, México

M. Galván-Arellano
Departamento de Ingeniería Eléctrica, SEES, CINVESTAV-IPN, Apartado Postal 14-740, México, D. F. 07000, México

have reported the LPE growth of $Ga_{1-x}In_xAs_{1-y}Sb_y$ on GaSb substrates with values of x as large as 0.22. This corresponds to a band gap of 0.53 eV (2.33 μm). This is a slight penetration into the predicted miscibility gap ($0.18<\times<0.84$) [2].

Among many techniques to grow $Ga_{1-x}In_xAs_ySb_{1-y}$ epitaxial layers on GaSb substrates, liquid phase epitaxy (LPE) still remains an attractive method due to its simplicity. But the existence of a large miscibility gap [3] hinders the $Ga_{1-x}In_xAs_ySb_{1-y}$ growth in a wide range of x and y values. It is considered a metastable alloy, with the tendency to decompose into regions of non-uniform alloy composition. It should be noted that, owing to the large unstable region, only GaSb-enriched solid solution compositions will be stable at typical LPE temperatures with lattice-matching to GaSb substrate [8]. This is why trying to reduce the band gap of the quaternary antimonide material for the desired value for TPV applications usually results in phase separations.

Photoluminescence spectroscopy is the most common characterization technique for investigating the distribution of defects, concerning the type and heavy doping effect in GaSb and its alloys, hence it was employed in this work. It is a non-destructive and noncontact technique for examining the band structure and luminescence properties of GaInAsSb. The alloy luminescence properties are dependent on the growth conditions (or methods), impurity species, doping concentrations, and growth temperatures. It has also been employed to investigate the Fermi level of heavily p-type doped materials [9], the carrier concentration [10], and the epitaxial layer quality [11]. We are reporting the luminescence properties of Zn-doped GaInAsSb with the varying Zn molar fraction for the first time. After thorough investigation of Zn-doped GaInAsSb, we have suggested a relationship of main energy emission band versus Zn molar fraction added to growth solution of Zn-doped GaInAsSb, which could be considered a useful tool to determine the free hole concentration in Zn-doped GaInAsSb by low temperature PL measurement. The hole concentration increases with increasing Zn molar fraction.

As photoluminescence, Raman spectroscopy has become increasingly popular in materials science and, especially, in semiconductor physics and microelectronics. Basically, Raman scattering probes the inelastic scattering of monochromatic light (incoming-photons) by the atomic vibrations in a medium (solid, liquid, or gas). In crystalline solids, the atomic vibrations are quantized (phonons), and they are very sensitive to internal and external perturbations, such as doping and stress. The frequency of the scattered light (outgoing photons) is then a local probe of the perturbation experienced (or not) by the medium. Today, the large number of results collected on semiconductors, combined with a good theoretical understanding of the scattering mechanisms, allows predicting reliably the effect of an external perturbation on the electronic and vibrational properties of the investigated medium (either ordered or disordered). Raman spectroscopy can then be used to identify the constituting species, study the compositional uniformity, crystallinity, doping level, and to probe locally the temperature and stress. At the industrial and investigation levels, Raman spectroscopy has become a very attractive characterization tool. This is because of its contactless and non-destructive nature. Thanks to recent turn-key Raman systems, one can perform repetitively large area mapping with spatial resolution down to 300 nm.

In this work, we report a systematic study and a quantitative evaluation of the effects of high Zn doping in $Ga_{0.86}In_{0.14}As_{0.13}Sb_{0.87}$ layers grown on (100) GaSb substrates by liquid phase epitaxy (LPE) using the Raman spectroscopy for determining the chemical compositional homogeneity and photoluminescence (PL) spectroscopy to obtain the optical properties.

2 Experimental Details

$Ga_{0.86}In_{0.14}As_{0.13}Sb_{0.87}$ epitaxial layers were grown in a three-zone furnace in a H_2-atmosphere, using a horizontal graphite sliding boat. As substrates, (100) GaSb wafers mechanically polished from Firebird, Inc. were used. All the precursor elements used to prepare the growth melt were of 6 N purity, and GaAs came from a wafer. For carrying out the intentional doping of the epilayers for high hole concentration zinc pellets were added in small quantities to the growth solution. After the charge of the substrate in the boat, the temperature was raised at 640 °C for 1 h, in order to eliminate the oxides in the substrate surface. Then, the temperature was decreased to stabilize the system, and a cooling ramp at a rate of about 0.3 °C/min was established, after the layers were grown at temperatures around 530 °C. Elemental chemical microanalysis measurements were performed using an FEI-Quanta 3D FEG model equipped with an X-ray dispersive energy microanalysis system (EDX). From the results obtained in the high resolution X-ray diffraction (HRXRD), measurements were obtained that the lattice mismatches between substrates and layers, ($\Delta a/a$), were of the order of 4.0×10^{-4} for all samples. The compositional homogeneity was verified by Raman spectroscopy, which was performed at room temperature in the near-backscattering geometry using the 6328 Å line of a He-Ne laser at normal incidence for excitation. The light was focused to a diameter of 6.0 μm at the sample using a ×50 (numerical aperture 0.9) microscope objective. The nominal laser power used in these measurements was 20 mW. Care was taken to avoid the heating of the sample inadvertently to the point of changing its Raman spectrum. Scattered light was analyzed using a micro-Raman system (Lambram model of Dilor), a holographic notch filter made by Kaiser Optical System, Inc. (model superNotch-Plus), a 256×1024-pixel CCD used as detector cooled to 140 K using liquid nitrogen,

and two interchangeable gratings (600 and 1800 g/mm). Typical spectrum acquisition time was limited to 60 s to minimize the sample heating effects. Photoluminescence measurements were carried out by exciting the sample with the 488 nm line of an Ar-ion laser, the excitation power was 120 mW and the measuring temperature was ~15 K with the sample enclosed in the cold finger of a closed-cycle He cryostat. For undoped sample photoluminescence, the excitation power was varied from 40 to 200 mW. Sample radiative emission was analyzed through an Acton monochromator and detected with an InSb infrared detector EG&G Judson cooled with liquid nitrogen. Assignation of each transition is accomplished studying the behavior of the PL spectra with the excitation power. The energy positions and the line width at half-maximum (FWHM) of each peak have been determined by a quantitative fit to the experimental PL spectra using a sum of Gaussian line distributions; the dominant peaks were fit first and the additional peaks were added as necessary. $Ga_{0.86}In_{0.14}As_{0.13}Sb_{0.87}$ layers with different zinc concentrations were grown by LPE by adding small quantities of Zn in the growth solution as is shown in Table 1.

3 Experimental Results and Discussion

The chemical composition of the typical sample CE164 is analyzed by EDX, which besides allows knowing the presence of any unintentional impurities. The CE164 EDX spectrum shows the presence of oxygen in the samples along with zinc, indium, antimony, gallium, and arsenic, see Fig. 1. It is widely accepted that oxygen is a residual impurity that introduces deep traps into III–V semiconductor compounds [12], which are dominant non-radiative deep centers located below the conduction band that critically reduce luminescence efficiency [12, 13]. Thus, it appears that oxygen has replaced antimony or arsenic at a few random points of the GaInAsSb lattice. The EDX spectrum indicates that, besides, the samples contain a significant amount of carbon. From EDX, characterization it was determined that the chemical stoichiometry of the quaternary layers, for all the samples, was approximately as follows: $Ga_{0.86}In_{0.14}As_{0.13}Sb_{0.87}$.

Table 1 Summary of the $Ga_{0.86}In_{0.14}As_{0.13}Sb_{0.87}$ samples studied in this work, which were grown by liquid phase epitaxy and besides Zn molar fraction added to each one is presented. All samples were grown at 530 °C on single crystal Te-doped GaSb substrates. The sample thicknesses were between 2 and 2.5 μm. Besides, it presents the hole concentrations estimated by low temperature photoluminescence measured at 15 K and at a laser power of 120 mW

Sample	Zn molar fraction	E_M (meV)	Concentration (cm^{-3})
CE135	Undoped	647.54	7.679×10^{16}
CE165	1.301×10^{-4}	641.95	5.095×10^{17}
CE163	1.711×10^{-4}	640.51	6.985×10^{17}
CE167	2.327×10^{-4}	639.95	7.717×10^{17}
CE157	3.284×10^{-4}	639.96	7.846×10^{17}
CE161	3.489×10^{-4}	637.88	1.149×10^{18}
CE164	5.337×10^{-4}	637.77	3.613×10^{18}
CE166	5.884×10^{-4}	634.79	4.484×10^{18}
CE148	6.773×10^{-4}	629.96	5.564×10^{18}

We made a map in some grown layers on different points of their surface morphology for verifying their chemical compositional homogeneity by Raman spectroscopy in the backscattering configuration, whose results are shown in Fig. 2a for a typical sample grown by LPE for this study. Figure 2b shows the deconvolution of two Raman spectra, which present the same bands that only vary in intensity. The vibrational bands observed in these Raman spectra have been discussed widely and published elsewhere [14]. Briefly, the Raman shifts of these vibrational modes in the quaternary alloys are modified with respect to their bulk values due to the effect of the internal stress originated on the difference in lattice constants between GaSb, InAs, and GaAs [15]. Taking into account that phonons are active in the first order Raman process in backscattering configuration on the (001) face, we may assign the vibrational bands observed around 217, 227, and 241 cm^{-1} to TO-(GaSb+InAs)-like, LO-(GaSb+InAs)-like, and LO-GaAs-like [16, 17] modes, respectively, which were obtained by deconvolution of Raman spectrum. Besides, the asymmetry of the GaAs-like mode is due to the contribution of the scattering process of phonons with non-zero **q**-vectors that become active due to the alloying disorder process [17, 18]. The TO-(GaSb+InAs)-like mode that is forbidden for the (100) orientation of the substrate becomes active by the breakdown of the selection rules in the backscattering configuration [19]. This breakdown is attributed to structural defects in the alloy originated from compositional fluctuations and by elastic scattering and by the ionized doping impurities [20]. As is observed in Fig. 2b, the samples' chemical homogeneity is very good and only presents small variations of the chemical composition.

Figure 3 shows the LT-PL spectrum of the sample CE135 measured at a laser power of 40 mW. An optical band gap energy of about 653 meV at 15 K has been estimated for this quaternary alloy [21]. As can be seen in Fig. 3, the dominant emission band has a slightly asymmetric shape in the sharp high-energy edge and the low-energy tail, which disappears with the increase of the excitation power. The quantitative fit of the dominant band of the 15 K PL spectrum measured at 40 mW suggests that the main radiative emission consists of three emission bands with photon energies centered at 640, 645, and 648 meV that have been associated to bound excitons labeled as BE_4, BE_2, and BE_1, respectively [22, 23]. These radiative emission bands can be associated with three different radiative recombination transitions, which have been associated with the radiative decay of excitons bound to

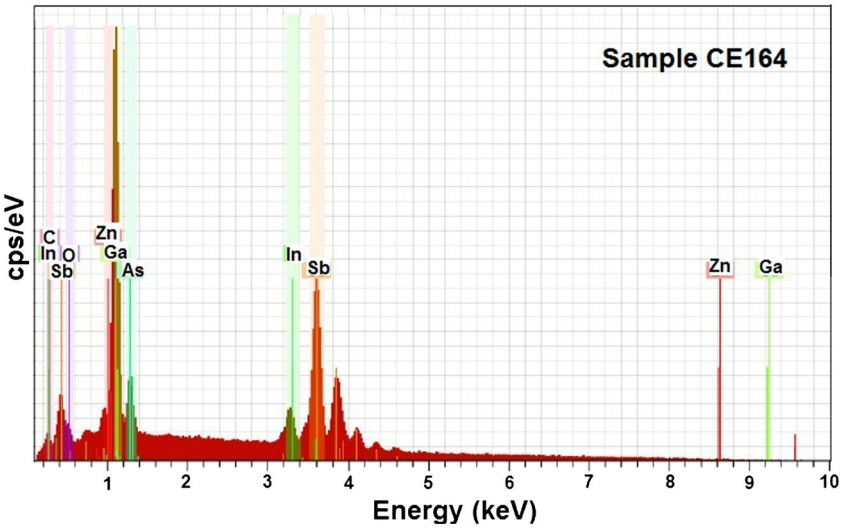

Fig. 1 Bulk EDX spectrum of $Ga_{0.86}In_{0.14}As_{0.13}Sb_{0.87}$ typical sample doped with zinc, the sample CE164 that is a typical sample doped with 5.337×10^{-4} of zinc molar fraction. The spectrum indicates that besides In, Ga, As, Sb, and Zn, the sample contains significant amounts of oxygen and carbon

neutral acceptor impurities. The origin of these acceptor impurities is not definitely known though some authors have conjectured that they are due to native defects. The transition BE_2 has been ascribed to the decay of an exciton bound to a dominant residual acceptor level that has a binding energy of 34–39 meV [23]. Very little is known about the acceptor impurity corresponding to the transition BE_1, while there are some conflicting reports concerning the origin of the transition BE_4. The values for the full width at half maximum (FWHM) of the main three PL bands at 40 mW of laser power are about 7.1, 4.2, and 9.2 meV, respectively. This fact indicates the good crystalline quality of the undoped $Ga_{0.86}In_{0.14}As_{0.13}Sb_{0.87}$ layer. The FWHM of the BE bands are smaller than or comparable to the best results previously reported on similar composition layers grown by LPE and other techniques [16]. Additionally to the excitonic transitions, a broad band is observed at low energy region that is constituted by acceptor-related transitions [16]. It is very well known that undoped GaSb and its alloys exhibit p-type conductivity caused by native defects such as V_{Ga} or $V_{Ga}Ga_{Sb}$

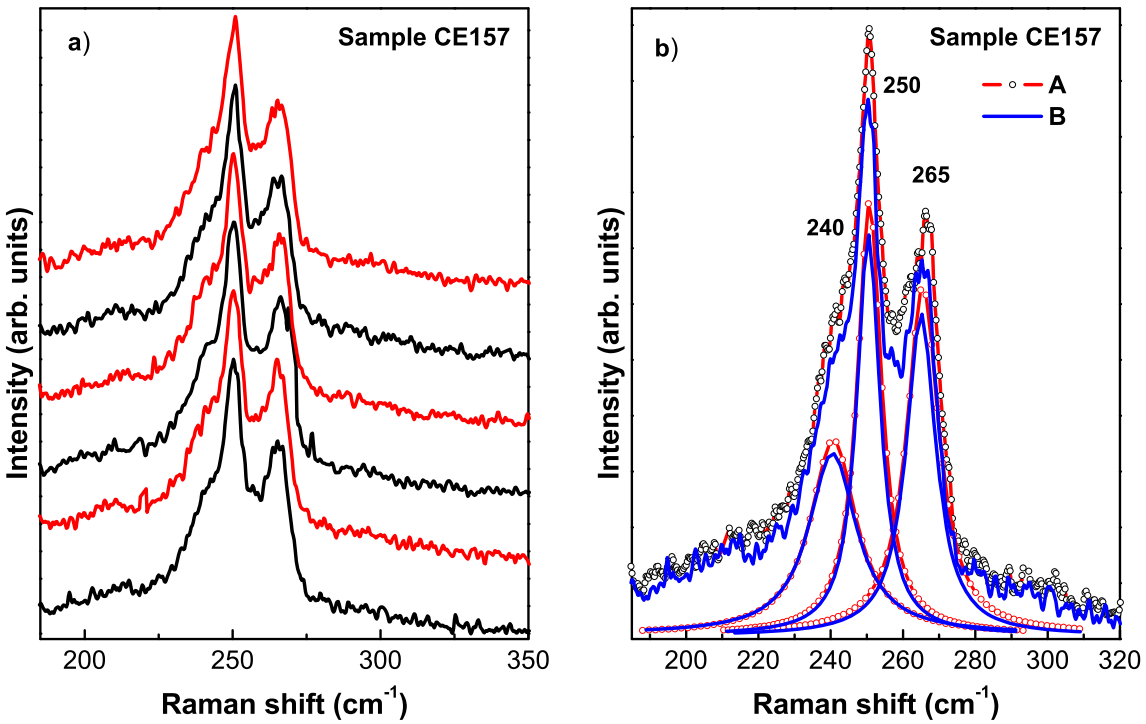

Fig. 2 **a** Raman spectra on different points of the same sample CE157 to verify the homogeneity of its chemical composition. **b** Deconvolution of two Raman spectra for showing that the same vibrational modes appear at the same Raman frequencies and only slightly vary their intensities, which were obtained at two different points on the surface, *A* and *B*

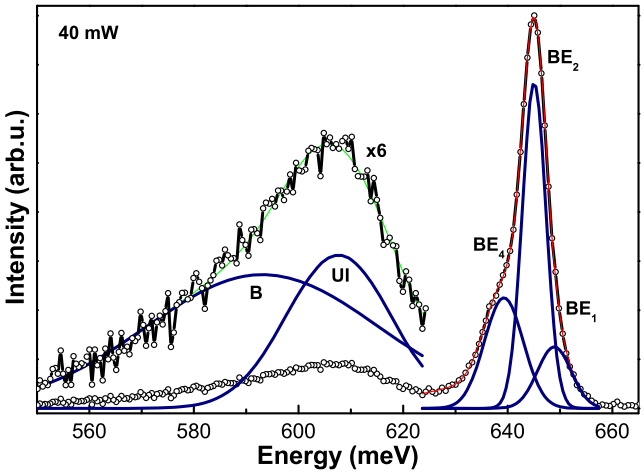

Fig. 3 Photoluminescence spectrum of undoped $Ga_{0.86}In_{0.14}As_{0.13}Sb_{0.87}$, sample CE135, measured at 15 K

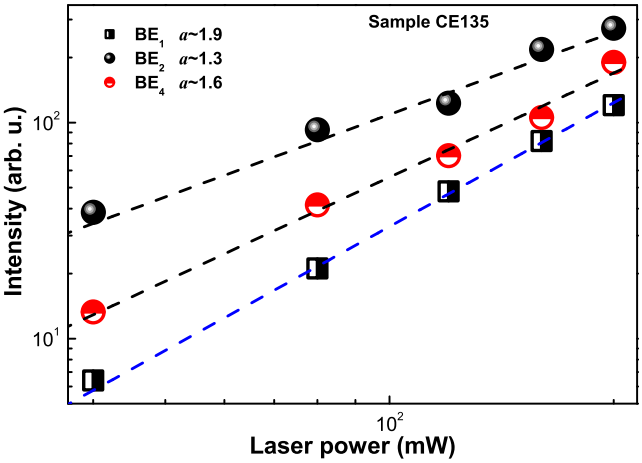

Fig. 4 Variation of PL band intensity of the sample CE135, which is not intentionally doped, as a function of the incident laser intensity

[24]. Generally, the lattice antisite defects $V_{Ga}Ga_{Sb}$ form double charged acceptor levels in the forbidden gap with activation energies (E_A) of 35 and 80 meV for the first and second ionized states, respectively. The emission band associated with radiative recombination transition to the first ionized state of the acceptor level is dominant in the PL spectra for GaInAsSb layers grown from stoichiometric melts. On the contrary, when using special melts, such as a lightly doped one, the exciton bound to donor and neutral acceptor transitions dominates, while the intensity of related band to native antisite defects is reduced. Then, the presence of impurities results in the appearance of radiative recombination through the acceptor level in the forbidden gap of the intentionally doped GaInAsSb solid solution. At the same time, the radiative recombination through the acceptor levels associated with $V_{Ga}Ga_{Sb}$ antisite native defects can be suppressed. Thus, the dominant exciton bound to neutral acceptor radiative transitions are typical for the PL spectra of undoped quaternary GaInAsSb solid solution, as was discussed above.

The photoluminescence of the sample CE135 was studied as a function of the incident laser power in the range from 40–200 mW to confirm the identification of the three radiative recombination transitions present in the 15 K PL spectra. Figure 4 shows the band intensities as a function of the excitation power; it is noteworthy that in the range of powers investigated, the luminescence of this sample did not show saturation. The intensity of the three radiative transitions as a function of incident laser power exhibits a dependence of P^a, with $a \sim 1.6$, 1.3, and 1.9, respectively. These values confirm that the three radiative transitions BE_4, BE_2, and BE_1 present in the 15 K-PL spectra are excitonic transitions [22]. The BE_1 excitonic transition energy presented a slight redshift as the incident laser power is increased. The other two excitonic transitions in the PL spectra did not shift remarkably their energy with the excitation power [25].

It is very interesting to consider the effect of zinc as group II dopant on the photoluminescence spectra of $Ga_{0.86}In_{0.14}As_{0.13}Sb_{0.87}$ solid solutions. Figure 5 illustrates the LT-PL emission spectra of GaInAsSb layers doped with different zinc molar fractions, which are shown in Table 1. The PL was measured at 15 K and an excitation power of 120 mW, because of at higher laser powers luminescence showed saturation, and at lower power excitation, luminescence signals were very noisy. The PL spectra were normalized to the same peak intensity and as is observed, all the samples' PL spectra exhibit one dominant emission. As is

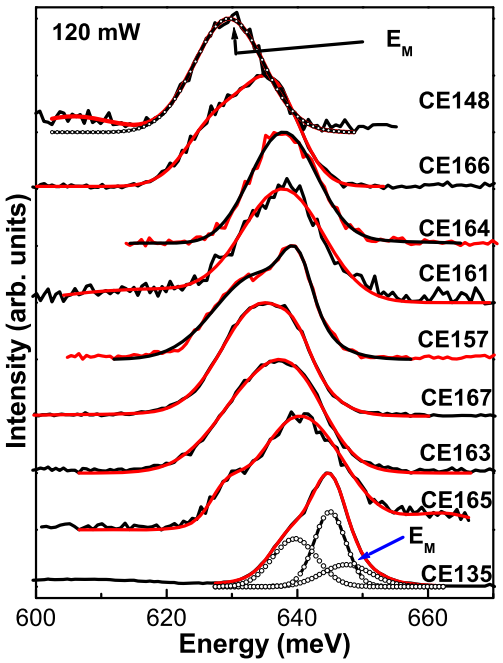

Fig. 5 Photoluminescence spectra of p-type $Ga_{0.86}In_{0.14}As_{0.13}Sb_{0.87}$ as a function of Zn concentration at 15 K for a laser power of 120 mW, *solid lines*. The *lines* (-o-o-) correspond to the components of the experimental LT-PL spectra obtained by deconvolution by Gaussian lines. In LT-PL spectra, the most energetic band is labeled by E_M

shown, zinc is an acceptor impurity in GaSb and its alloys, which means that Zn atoms as substitutional impurities can substitute Ga atoms in the GaSb sublattice since the covalent radius of Zn atom (a_{Zn}=0.125 nm) is nearly the same as that of Ga atom (a_{Ga}=0.126 nm). The influence of the doping by zinc for wide regimen on the optical properties was studied using the low-temperature photoluminescence.

At low p-type doping concentration, the acceptor impurity energy could be treated as a δ function. The low-temperature photoluminescence spectrum of the non-degenerate semiconductor materials could be explained by band-to-band (BB) and band-to-acceptor (BA) radiative transitions, as schematically illustrated in Fig. 6a. As p-type dopant concentration is increased, the dopant level spreads into a band on two sides. The heavier the doping, the more the spread, as evidenced from the increase of the FWHM with the increase in dopant concentration incorporated in the layers [26]. However, as the doping concentration is further increased to a level comparable to the effective density of states in the valence band, the most energetic band (E_M) starts shifting toward the low energy side. An example is schematically shown in Fig. 6b.

As the p-type dopant concentration is increased in the crystal, the average spacing of the impurity atoms becomes smaller. When this is close to or less than the Bohr radius of the impurity states, the majority carriers in the crystal become so numerous that their presence alters the lattice periodic potential. As a result of the high carrier concentration, three effects should be considered for studying the physical properties of the crystal. One of them is many-body effects that involve ionized acceptor-hole interaction, hole-hole interaction, and electron-hole interaction. The ionized acceptor-hole interaction gives as a result a reduction in the acceptor ionization energy and causes the acceptor level to move toward the valence band edge Ev. The hole-hole interaction shifts Ev upward. The electron-hole coulomb interaction reduces the electron potential energy and causes the conduction band edge

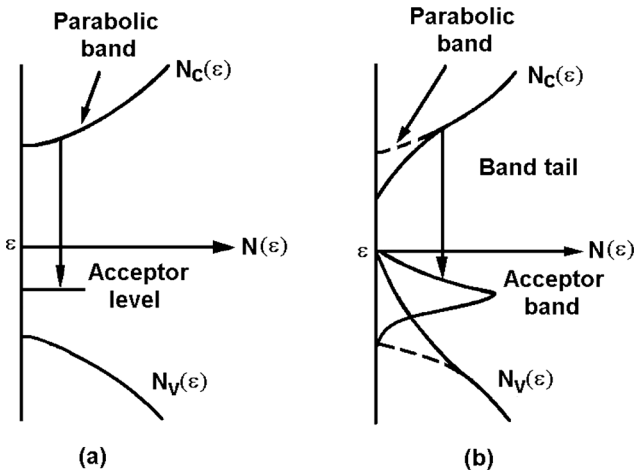

Fig. 6 Schematic illustration of photoluminescence emission from **a** slightly doped and **b** heavily doped sample

to move down. The second effect that should be considered is the randomness of the Zn atoms that causes fluctuations in the local electrostatic potential and results in the formation of band tail states. Finally, the effect of the carrier degeneracy should also be considered as the Maxwell-Boltzmann statistics will be replaced by the Fermi-Dirac statistics in the case of degenerate semiconductors.

As can be seen in Fig. 5, the main radiative band labeled by E_M in the LT-PL spectra shifts toward lower energies (redshift) as the Zn molar fraction is increased in growth solution from 0 to 6.773×10^{-4} M. The shift of the photoluminescence spectra toward the low energy side with the increase in Zn concentration shown in Fig. 5 could be well explained by the above theory. This redshift indicates that the LT-PL spectra come from the direct band-to-band or direct impurity-to-band transitions following the k conserving rule. The spectral shape of the PL emission band is almost symmetric. The asymmetry of the spectrum observed at higher Zn molar fraction, sample CE166, in Fig. 5 strongly indicates that effective band-to-band or effective band-to-acceptor transitions dominate the emission across the energy gap breaking the k conservation [27, 28]. The steep slope characterized by the exponential decay, $\exp(\hbar\omega/E_t)$ of the luminescence on the high-energy side is caused by a decrease in the hole population below the Fermi energy levels, whereas the smooth slope on the low-energy side closely follows the relationship, $I\propto(E_t-\hbar\omega)^{1/2}$ [29] where E_t is the threshold energy of band in Fig. 5 and I is the spectral intensity at the photon energy $\hbar\omega$. In Table 1, the results of the energetic position of the band E_M obtained by deconvolution of the LT-PL spectra of the studied samples are shown.

Using the results of the energy position of the band E_M for high levels of zinc concentration, one may estimate the majority carriers concentration that show a good agreement with the results obtained with the SIMS measurement [30]; in order to do this, it is necessary to include not only the usual band filling effect but also the band gap shrinkage due to the exchange interaction among free carriers as well as the band tailing effect due to the Coulomb interaction of the free carriers with ionized impurities. All the above mentioned interactions are calculated taking into account the non-parabolicity of the valence band which results in a concentration dependent effective mass. It is assumed that the hole distribution is degenerate, whereas the electrons introduced by optical generation occupy the states at the very bottom of the conduction band. Therefore, to a good approximation, the peak of the photoluminescence band E_M arising from band-to-band (BB) transitions would be given by [31]:

$$E_M(p) = E_{g0} + E_F'(p) + E_C^h(p) - E_C^{C'}(p), \quad (1)$$

where E_{g0}, E_F', E_C^h and $E_C^{C'}$ are as follows: the band gap of undoped GaInAsSb at 15 K, the Fermi energy for non-

parabolic bands, the hole–impurity interaction, and the exchange interaction among free carriers, respectively. This equation can be used to estimate the hole concentration in the samples, in fast form and without using a destructive technique. Here, it has been supposed that Eq. (1) might also be valid at low zinc concentration to estimate the hole concentration in the whole investigated range. The hole concentration was obtained through the adjustment of the main PL peak with the band-filling model, Eq. (1), which takes into account the shift of the Fermi energy toward the valence band as the acceptor concentration increases. These results suggest that the Zn atoms incorporate in the samples as acceptor impurities. The obtained results are presented in Table 1 and in Fig. 7, which are in agreement with the published results [32].

In the light of the above interpretations, it might be concluded that in the Zn molar fraction range up to 3.49×10^{-4} M, a downward shift of the photoluminescence peak is observed due to the predominance of band shrinkage resulting from combined exchange and Coulomb interactions over the band filling. The low temperature PL spectra in this Zn molar fraction range can be explained in terms of direct k-conserving transitions. For higher Zn molar fraction, which corresponds to degenerate concentrations, however, it is properly interpreted in terms of non-k-conserving transitions which arise from indirect recombination of holes in a highly filled valence band.

Figure 8 shows the band gap narrowing (BGN) values of GaInAsSb layers obtained experimentally from low temperature photoluminescence measurements versus the hole concentration estimated by Eq. (1), which are adjusted by means of the following equation [33]:

$$\Delta E_g(p) = Ap^{1/3} + Bp^{1/4} + Cp^{1/2}. \quad (2)$$

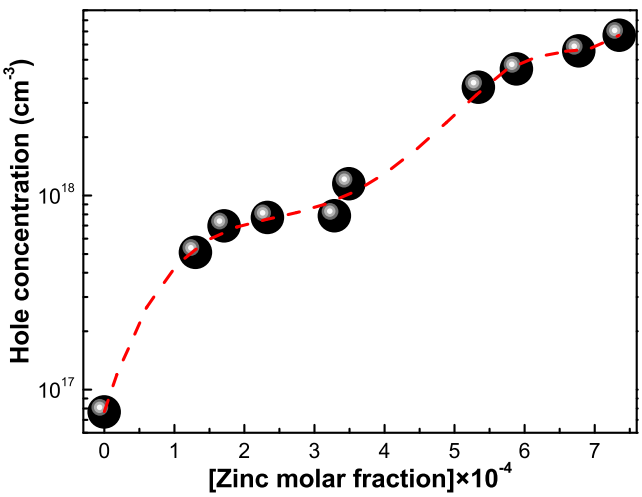

Fig. 7 Hole concentration as a function of the zinc molar fraction in the quaternary $Ga_{0.86}In_{0.14}As_{0.13}Sb_{0.87}$: Zn epitaxial layers obtained for excitation power of 120 Mw and a temperature of 15 K

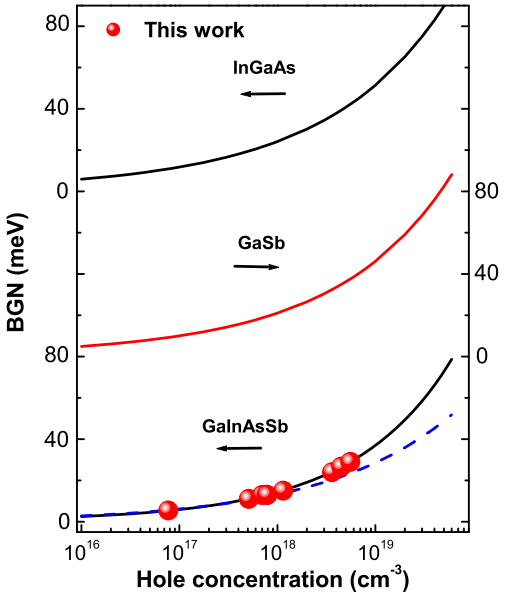

Fig. 8 From *top to bottom*, predicted BGN p-type InGaAs, GaSb, and GaInAsSb. The *solid line* corresponds to Eq. (2). *Dashed line* is the fit to $a\times p^{1/3}$. *Closed circles* correspond to the $Ga_{0.86}In_{0.14}As_{0.13}Sb_{0.87}$ E_M measurements at 15 K

Besides, as is observed in Fig. 8, BGN may be fitted successfully to the equation in the range of investigated Zn molar fraction that is represented by the solid line, with parameters as follows: $A=3.03603\times10^{-6}$, $B=1.3\times10^{-4}$, and $C=7.42865\times10^{-9}$. In addition, it adjusted the BGN to $\Delta E_g(p)=a\times p^{1/3}$; the relation is plotted and it is shown in the figure, which is not very good due to the fact that this relation is valid for concentrations higher than 10^{18} cm^{-3}. In Fig. 8 the dashed line corresponds to the $p^{1/3}$ fit, where $a=1.3249\times10^{-5}$. Additionally, the GaInAsSb BGN values are compared to BNG values reported by Jaen et al., finding a good agreement with the experimental data as can be seen in Fig. 8.

4 Conclusions

To summarize, in this work, we presented a systematic study of doping by zinc in $Ga_{0.86}In_{0.14}As_{0.13}Sb_{0.87}$ epitaxial layers grown on (100) GaSb substrates by LPE. The studied epilayers were doped with Zn in a broad range from low to high concentrations. The chemical stoichiometry of the epilayers is roughly $In_{0.14}Ga_{0.86}As_{0.13}Sb_{0.87}$ and was determined by measurements of X-ray dispersive energy microanalysis system (EDX). The compositional homogeneity was found by Raman scattering, which shows two phononic bands that may be assigned to the GaAs-like and (GaSb+InAs)-like mixture modes. For low doping levels, the PL spectra show the presence of exciton-related transitions with a small FWHM value (7 meV), which is evidence of good crystalline quality of the layer. For higher doping levels, the PL spectra

exhibit band-to-band and donor-to-acceptor transitions which merge in a broad band as the Zn doping increases. An important result of the analysis is that nonparabolicity of the valence band has to be taken into account in calculating the peak position of photoluminescence spectra at degenerate concentrations and in estimating the hole concentration for the grown samples. The predictive model for band gap narrowing has been applied to GaInAsSb, which is in good agreement with experimental results.

References

1. D. C. Tran. G. H. Siegel. Jr., B. Bendow. Lightwave Technol. (Special Issue on Low-Loss Fibers) **LT-2** (1984) 536.
2. G.B. Stringfellow, J. Cryst. Growth **58**, 194 (1982)
3. K. Nakajima, K. Osamura, K. Yasuda, Y. Murakami, J. Cryst. Growth **41**, 87 (1977)
4. M. Dolginov, D.G. Elisev, A.N. Lapshin, M.G. Milvidskii, Krist. Tech. **13**, 631 (1978)
5. N. Kobayashi, Y. Horikoshi, C. Uemura, Jpn. J. Appl. Phys. **18**, 2169 (1979)
6. H. Kano, S. Miyazawa, K. Sugiyama, Jpn. J. Appl. Phys. **18**, 21B3 (1979)
7. J.C. DeWinter, M.A. Pollack, A.K. Srivastava, J.L. Zyskind, J. Electron. Mater. **14**, 729 (1985)
8. J.L. Lazzari, E. Tournié, F. Pitard, A. Joullié, Mat. Sci. Eng. B **9**, 125 (1991)
9. J. Nagle, R.J. Malik, D. Gershoni, J. Cryst. Growth **111**, 264 (1991)
10. L.W. Yang, P.D. Wright, V. Eu, Z.H. Lu, A. Majerfeld, J. Appl. Phys. **72**, 2063 (1992)
11. S.I. Kim, M.S. Kim, Y. Kim, K.S. Eom, S.K. Min, C. Lee, J. Appl. Phys. **73**, 4703 (1993)
12. P.K. Bhattacharya, T. Matsumoto, S. Subramanian, J. Cryst. Growth **68**, 301 (1984)
13. T. Nakanisi, J. Cryst. Growth **68**, 282 (1984)
14. J. Díaz-Reyes, J.G. Mendoza-Álvarez, P. Rodríguez-Fragoso, E. López-Cruz, J.L. Herrera-Pérez, Vib. Spectrosc. **68**, 109 (2013)
15. J. Menendez, A. Pinczuk, J. Bevk, J.P. Mannaerts, J. Vac. Sci. Technol. B **6**, 1306 (1988)
16. F. Frost, G. Lippold, A. Schindler, F. Bigl, J. Appl. Phys. **85**, 8378 (1999)
17. T.C. McGlinn, T.N. Krabach, M.V. Klein, G. Bajor, J.E. Greene, B. Kramer, S.A. Barnett, A. Lastras, S. Gorbatkin, Phys. Rev. B **33**, 8396 (1986)
18. D.H. Jaw, Y.T. Cherng, G.B. Stringfellow, J. Appl. Phys. **66**, 1965 (1989)
19. R. Loudon, Adv. Phys. **13**, 423 (1964)
20. D. Olego, M. Cardona, Phys. Rev. B **24**, 7217 (1981)
21. J. Díaz-Reyes, J.A. Cardona-Bedoya, M.L. Gómez-Herrera, J.L. Herrera-Pérez, I. Riech, J.G. Mendoza-Alvarez, J. Phys. Condens. Matter **15**, 8941 (2003)
22. S. Iyer, S. Hegde, A. Abul-Fadl, W. Mitchel, Phys. Rev. B **47**, 1329 (1993)
23. E.T.R. Chidley, S.K. Haywood, A.B. Henriques, N.J. Mason, R.J. Nicholas, P.J. Walker, Semicond. Sci. Technol. **6**, 45 (1991)
24. M. Ichimura, K. Higuchi, Y. Hattori, T. Wada, N. Kitamura, J. Appl. Phys. **68**, 6153 (1990)
25. J. Díaz-Reyes, M.L. Gomez-Herrera, J.L. Herrera-Pérez, P. Rodríguez, J.G. Mendoza-Álvarez, Cryst. Growth Des. **9**, 3477 (2009)
26. G.B. Scott, G. Duggan, P. Dawson, G. Weimann, J. Appl. Phys. **52**, 6888 (1981)
27. C.W. Chen, M.C. Wu, S.C. Lu, C.C. Chang, Jpn. J. Appl. Phys. 1 **32**, 2725 (1993)
28. J. De-Sheng, Y. Makita, K. Ploog, H.J. Quisser, Ploog, H.J. Queisser. J. Appl. Phys. **53**, 999 (1982)
29. H. Barry, E.W. Williams, in: R. K. Willardson, A. C. Beer (Eds.), Semiconductors and Semimetals, Vol. 8, Academic, New York, 1972. (Chapter. 5).
30. Y.E. Bravo-García, M. Zapata-Torres, P. Rodríguez-Fragoso, J.G. Mendoza-Álvarez, J.L. Herrera-Pérez, J.A. Cardona- Bedoya, M.L. Gómez-Herrera, Superficies y Vacío **25**, 175 (2012)
31. J. Díaz-Reyes, P. Rodríguez-Fragoso, J.G. Mendoza-Álvarez, J. Lumin. **134**, 126 (2013)
32. R.M. Biefeld, J.G. Cederberg, G.M. Peake, S.R. Kurtz, J. Cryst. Growth **225**, 384 (2001)
33. S.C. Jain, J.M. McGregor, D.J. Roulston, J. Appl. Phys. **68**, 3747 (1990)